ISSN 1063-7826, Semiconductors, 2014, Vol. 48, No. 1, pp. 83–88. © Pleiades Publishing, Ltd., 2014.
Original Russian Text © A.A. Afonenko, D.V. Ushakov, 2014, published in Fizika i Tekhnika Poluprovodnikov, 2014, Vol. 48, No. 1, pp. 88–93.

MATERIALS OF THE 3rd SYMPOSIUM "SEMICONDUCTOR LASERS: PHYSICS AND TECHNOLOGY" (ST. PETERSBURG, OCTOBER 13–16, 2012)

Current-Injection Efficiency in Semiconductor Lasers with a Waveguide Based on Quantum Wells

A. A. Afonenko^ and D. V. Ushakov

Belarusian State University, Minsk, 220030 Belarus

^e-mail: afonenko@bsu.by

Submitted June 1, 2013; accepted for publication June 16, 2013

Abstract—A dynamic distributed diffusion–drift model of laser heterostructures, which takes into account carrier capture by quantum wells, is developed. The leakage currents in the lasing mode are calculated for different laser structures without wide-gap emitters: InGaAs/GaAs (lasing wavelength $\lambda = 0.98$ μm), InGaAsP/InP ($\lambda = 1.3$ μm), and InGaAs/InP ($\lambda = 1.55$ μm). It is shown that consideration of the finite carrier-capture time is of major importance for calculating structures with deep quantum wells. The ratio of the leakage currents to the total current in the structures with deep quantum wells (InGaAsP/InP and InGaAs/InP) increases with an increase in the injection current and may reach a few percent when the lasing threshold is multiply exceeded.

DOI: 10.1134/S1063782614010023

1. INTRODUCTION

Lasers with quantum wells (QWs) allow one to design a waveguide using the difference in the refractive indices of the QW material and the surrounding semiconductor. Although the QW width is small in comparison with the lasing wavelength, preliminary calculations showed that a small number (3–6) of quantum wells are sufficient to form a waveguide [1]. In this case, the characteristic mode-localization length in the direction perpendicular to the QW plane is about 1 μm (i.e., corresponds to a very wide waveguide). However, in contrast to very wide waveguides, there are no problems with mode selection in this design.

The lack of wide-gap emitters in these structures leads to the absence of built-in potential barriers in the bands, which hinder the diffusion of nonequilibrium carriers from the active region. Due to this, the leakage currents may significantly increase and the injection efficiency may fall, as occurs in separate-confinement lasers upon the introduction of an extended waveguide [2]. In this case, slowed carrier capture by the QW and electron leakage from the active region into the waveguide become important factors [2, 3].

The purpose of this study is to modify the standard heterostructure diffusion–drift model [4–6] to take into consideration the processes of carrier capture–ejection to QW levels and estimate the injection efficiency of different laser heterostructures without wide-gap emitters: InGaAs/GaAs (lasing wavelength $\lambda = 0.98$ μm), InGaAsP/InP ($\lambda = 1.3$ μm), and InGaAs/InP ($\lambda = 1.55$ μm).

2. THEORETICAL MODEL

2.1. Distributed Model

Within the distributed model, each point in space is characterized by three variables (for example, the electrostatic potential φ and Fermi quasi-levels for electrons (F_n) and holes (F_p)) [7]. They can be found by combined numerical integration of the fundamental system of equations, consisting of the Poisson equation for the electrostatic potential φ and the continuity equations for the electron (j_n) and hole (j_p) current densities:

$$\frac{d^2\varphi}{dz^2} = -\frac{e}{\varepsilon\varepsilon_0}(p - n + N_d - N_a), \quad (1)$$

$$\frac{1}{e}\frac{\partial j_n}{\partial z} = R + v_g G S_{3D} + \frac{\partial n}{\partial t}, \quad j_n = \mu_n n_b \frac{\partial F_n}{\partial z}, \quad (2)$$

$$\frac{1}{e}\frac{\partial j_p}{\partial z} = -R - v_g G S_{3D} - \frac{\partial p}{\partial t}, \quad j_p = \mu_p p_b \frac{\partial F_p}{\partial z}, \quad (3)$$

where n and p are the electron and hole concentrations, respectively; N_a and N_d are the concentrations of ionized acceptors and donors, respectively; ε is the permittivity; ε_0 is the dielectric constant; R is the recombination rate; G is the gain; S_{3D} is the bulk photon density; v_g is the group velocity; and μ_n and μ_p are, respectively, the electron and hole mobilities. The total

electron (n) and hole (p) concentrations include the concentrations of nonlocalized carriers (n_b and p_b, respectively),

$$n_b = N_c\Phi_{1/2}\left(\frac{F_n - E_c}{kT}\right), \quad p_b = N_v\Phi_{1/2}\left(\frac{E_v - F_p}{kT}\right), \quad (4)$$

which participate in charge transfer, and the concentrations of carriers localized at the QW levels (n_w and p_w, respectively),

$$n_w = N_{wc}\sum_i \ln\left[1 + \exp\left(\frac{F_n - \Delta F_{wn} - E_{ci}}{kT}\right)\right] \times \frac{2}{d}\sin^2\left(\frac{i\pi z}{d}\right), \quad (5)$$

$$p_w = \sum_i N_{wvi}\ln\left[1 + \exp\left(\frac{E_{vi} - F_p - \Delta F_{wp}}{kT}\right)\right] \times \frac{2}{d}\sin^2\left(\frac{\pi z}{d}\right). \quad (6)$$

Here, N_c (N_{wc}) and N_v (N_{wv}) are the bulk (two-dimensional) effective electron and hole densities of states, respectively; T is temperature; and k is the Boltzmann constant; the z coordinate is counted from the beginning of the quantum-well layer with a thickness of d. The hole concentration was calculated with allowance for the light- and heavy-hole subbands. The effective densities of states and the energy levels E_{ci} and E_{vi} were calculated within the effective-mass approximation. The parameters ΔF_{wn} and ΔF_{wp} take into account the finite times of carrier capture at the QW levels. Within the approximation of fast intraband relaxation these values are zero.

The energies of the bottom of the conduction band (E_c) and top of the valence band (E_v) were found using the electron affinity χ and the band gap E_g of the semiconductor layers:

$$E_c = -\chi - \varphi, \quad E_v = -\chi - E_g - \varphi. \quad (7)$$

The χ value in the QWs was chosen so as to correlate with the experimental data on the band discontinuities [8]. To calculate the concentrations of nonlocalized carriers in the QWs, we used formulas (4), where the energies E_c and E_v were assumed to be equal to the corresponding values for the adjacent barrier layers.

The spontaneous recombination rate was calculated within the direct-transition model from the approximate formula

$$R = A_{cv}\frac{N_r}{N_cN_v}\frac{np}{1 + (N_r/N_cN_v)(n+p)}. \quad (8)$$

Here, A_{cv} is the Einstein coefficient for spontaneous transitions and N_r is the reduced effective density of states. For QWs we applied similar formula with additional summation over the subbands, taking into account their occupancy. The gain G was calculated within the direct-transition model. Spectral-broadening effects were taken into consideration by formal replacement of the Heaviside function with a smoothed step function [9].

2.2. Boundary Conditions

The thicknesses of the emitter layers were chosen to be much larger than the screening length in these layers, which made it possible to construct the boundary conditions for the Poisson equation based on the electroneutrality condition:

$$(p - n + N_d - N_a)\big|_{P,N} = 0. \quad (9)$$

Here, the subscripts N and P indicate the external boundaries of the corresponding emitters. The boundary conditions for the continuity equations were chosen to be

$$F_p\big|_P = 0, \quad F_n\big|_N = U, \quad (10)$$

where U is the voltage applied to the structure. In the dynamic mode,

$$\frac{\partial U}{\partial t} = \int_P^N \frac{j - j_n - j_p}{\varepsilon_0\varepsilon}dz, \quad (11)$$

where j is the total current density through the structure. The minority-carrier transport into the bulk of the emitter layers (leakage currents) was assumed to be mainly diffusive; i.e., we used the following conditions:

$$\left.\frac{dj_n}{dz}\right|_P = \kappa_n j_n, \quad \kappa_n = \sqrt{\frac{e}{kT\mu_n\tau_n}}, \quad \frac{1}{\tau_n} = \left.\frac{\partial R}{\partial n}\right|_P, \quad (12)$$

$$\left.\frac{dj_p}{dz}\right|_N = -\kappa_p j_p, \quad \kappa_p = \sqrt{\frac{e}{kT\mu_p\tau_p}}, \quad \frac{1}{\tau_p} = \left.\frac{\partial R}{\partial n}\right|_N, \quad (13)$$

where κ_n (τ_n) and κ_p (τ_p) are the inverse diffusion lengths (lifetimes) of minority carriers.

2.3. Lasing Dynamics

The bulk photon density near the mth QW was calculated as

$$S_{3Dm} = \frac{\Gamma_m S_{2D}}{d_m}, \quad (14)$$

where Γ_m is the optical-confinement factor and d_m is the QW width. The dynamics of the two-dimensional

Table 1. Calculation parameters

Parameter	GaAs	$Ga_{0.8}In_{0.2}As$	InP	$Ga_{0.7}In_{0.3}As_{0.65}P_{0.35}$	$In_{0.53}Ga_{0.47}As$
E_g(300 K), eV	1.422	1.131	1.353	0.904	0.734
m_c/m_e	0.062	0.053	0.075	0.048	0.041
m_{vl}/m_e	0.090	0.061	0.121	0.046	0.040
m_{vh}/m_e	0.350	0.346	0.532	0.370	0.341
m_{vlt}/m_e	0.203	0.160	0.287	0.135	0.119
m_{vht}/m_e	0.111	0.077	0.150	0.059	0.052
ΔE_c, meV	0	166	0	157.5	250

m_e is the free-electron mass.

photon density S_{2D} was described by the standard rate equation

$$\frac{dS_{2D}}{dt} = v_g\left(\frac{\sum_m G_m}{1+\varepsilon_s S_{2D}} - k_{th}\right)S_{2D} + \beta\sum_m R_m, \qquad (15)$$

where G_m is the mean gain in the mth QW, R_m is the two-dimensional spontaneous recombination rate in the mth QW, ε_s is the nonlinear gain factor, β is the contribution of spontaneous transitions to the laser mode, and k_{th} is the threshold gain. Summation is performed over all QWs.

2.4. Carrier Capture by QWs

When the processes of carrier capture and ejection to QW levels have finite rates, the quasi-equilibrium between the carriers localized and nonlocalized in the QWs is violated, which limits the range of applicability of the conventional distributed model. This problem can be solved by increasing the number of variables characterizing one point in space; to this end, additional Fermi levels for localized electrons and holes are introduced into the QW regions. However, this procedure increases the size of the calculated matrices and reduces the convergence rate. In addition, carrier capture is not local in the physical sense; i.e., carriers captured at any point above the QW are distributed over the entire QW.

The simplest way to solve the aforementioned problem is self-consistent solution of the fundamental system of equations and the system of balance equations, where the rates of carrier capture at localized levels are equated with the interband-recombination rates in the QWs:

$$0 = \int_w\left\{\frac{n_b}{\tau_{cn}}\left[1-\exp\left(-\frac{\Delta F_{wn}}{kT}\right)\right] - R_w - v_g G S_{3D} - \frac{\partial n_w}{\partial t}\right\}dz, \qquad (16)$$

$$0 = \int_w\left\{\frac{n_b}{\tau_{cp}}\left[1-\exp\left(-\frac{\Delta F_{wp}}{kT}\right)\right] - R_w - v_g G S_{3D} - \frac{\partial p_w}{\partial t}\right\}dz. \qquad (17)$$

Here, τ_{cn} and τ_{cp} are, respectively, the times of electron and hole capture by an unoccupied QW; the exponential terms in parentheses allow for the change in the effective capture time upon QW-level filling; and integration is performed separately for each QW. Although only two calculated parameters ΔF_{wn} and ΔF_{wp} are added for each QW within the model under consideration, this approach makes it possible to introduce different Fermi quasi-levels for each QW subband (as in calculations of intrasubband-transition lasers [10]).

The probability of free-carrier capture by a QW heavily depends on the energy position of the highest bound state in the QW (it is maximum when this state is virtual [11–13]). The times of carrier capture by the QW in InGaAs/GaAs heterostructures were measured in [14] (based on photoluminescence analysis) to be 1 and 6.5 ps at 300 and 10 K, respectively.

2.5. Solution Algorithm

Our calculations of different quantum-well structures showed that the coupled iterative solution to the system of equations (1)–(3) and (15)–(17) in the steady-state mode is not convergent under strong inhomogeneous excitation of the QWs and for high barrier regions ($\Delta F_{wn}, \Delta F_{wp} > kT$). A possible reason is the existence of many steady-state solutions to the nonlinear system of basic equations. This problem can be solved by the consideration of lasing dynamics.

The time sampling of all equations was performed by the implicit Euler method. The fundamental system of equations (1)–(3) was solved using the finite-difference scheme. Joint self-consistent solution of the fundamental system of equations and Eqs. (11) and (15)–(17) was performed by the iterative method. The following algorithm, consisting of two embedded

Table 2. Electron and hole mobilities in the emitter layers

Mobility	GaAs		InP	
	$N_a = 10^{18}$ cm^{-3}	$N_d = 5 \times 10^{17}$ cm^{-3}	$N_a = 10^{18}$ cm^{-3}	$N_d = 5 \times 10^{17}$ cm^{-3}
μ_n, cm^2 V^{-1} s^{-1}	2200	5800	1480	3070
μ_p, cm^2 V^{-1} s^{-1}	60	370	45	170

iterative loops, was found to be the most efficient. The internal loop included the successive solution of Eq. (14) for the photon density S_{2D}, Eqs. (16) and (17) for the pairs of parameters ΔF_{wnm} and ΔF_{wpm} for each (mth) QW, and the Poisson equation (1) for the electrostatic potential φ. The external loop included the internal loop, continuity equations (2) and (3) for the Fermi quasi-levels for electrons (F_n) and holes (F_p), and Eq. (11) for the voltage U. The F_n, F_p, and U values were calculated by the under-relaxation method. To provide solution convergence, the time integration step could be varied from several tens to several tenths of a picosecond. The obtained systems of nonlinear equations were solved by the Newton method.

3. NUMERICAL CALCULATION AND RESULTS

The parameters of the numerical calculation (band gap E_g and effective electron (m_c) and hole (m_{vl}, m_{vh},

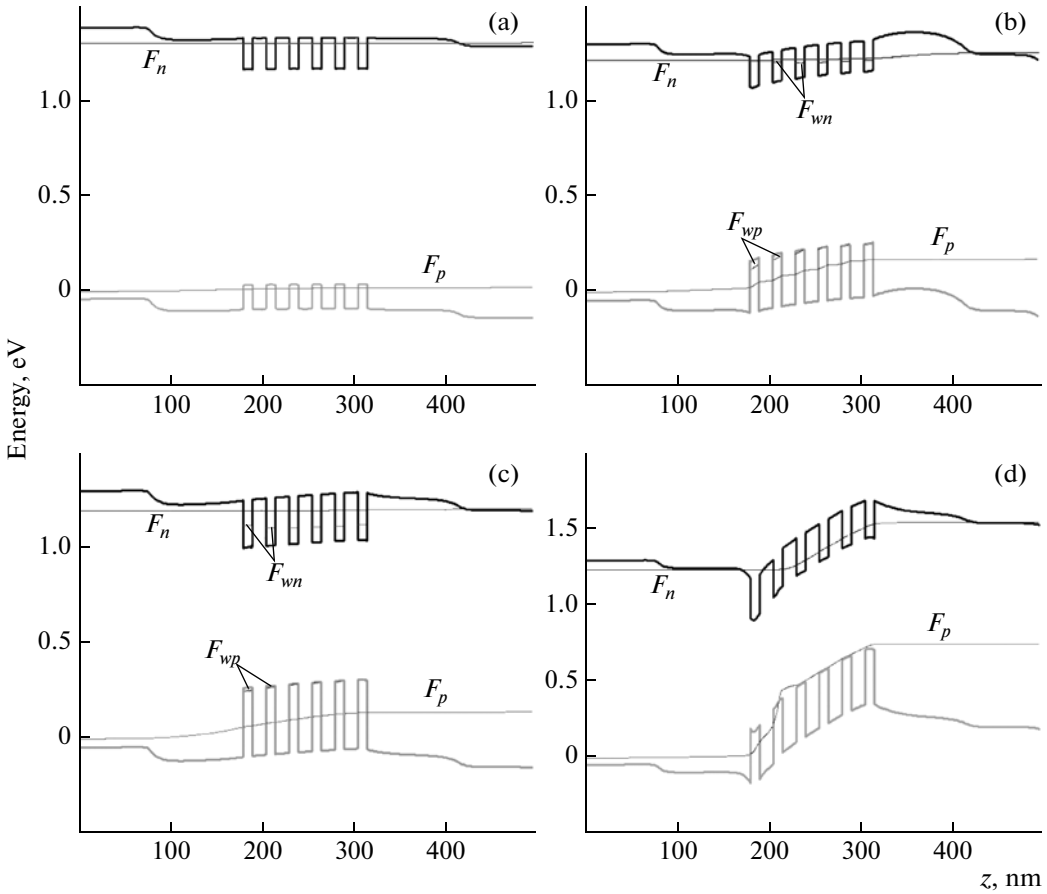

Fig. 1. Energy band diagrams of the heterostructures at $j = 10$ kA/cm^2 for the following systems: (a) $Ga_{0.8}In_{0.2}As/GaAs$ ($U = 1.306$ V, $S_{2D} = 1.2 \times 10^{11}$ cm^{-2}, $\tau_{cn} = \tau_{cp} = 1$ ps), (b) $Ga_{0.7}In_{0.3}As_{0.65}P_{0.35}/InP$ ($U = 1.255$ V, $S_{2D} = 1.3 \times 10^{11}$ cm^{-2}, $\tau_{cn} = \tau_{cp} = 1$ ps), (c) $Ga_{0.47}In_{0.53}As/InP$ ($U = 1.207$ V, $S_{2D} = 1.5 \times 10^{11}$ cm^{-2}, $\tau_{cn} = \tau_{cp} = 1$ ps), and (d) $Ga_{0.47}In_{0.53}As/InP$ ($U = 1.556$ V, $S_{2D} = 1.1 \times 10^{11}$ cm^{-2}, $\tau_{cn} = \tau_{cp} = 0$ ps). The bottom of the conduction band; the top of the valence band; and the Fermi quasi-levels for nonlocalized (F_n and F_p) and localized ($F_{wn} = F_n - \Delta F_{wn}$ and $F_{wp} = F_p + \Delta F_{wp}$) electrons and holes, respectively, are indicated.

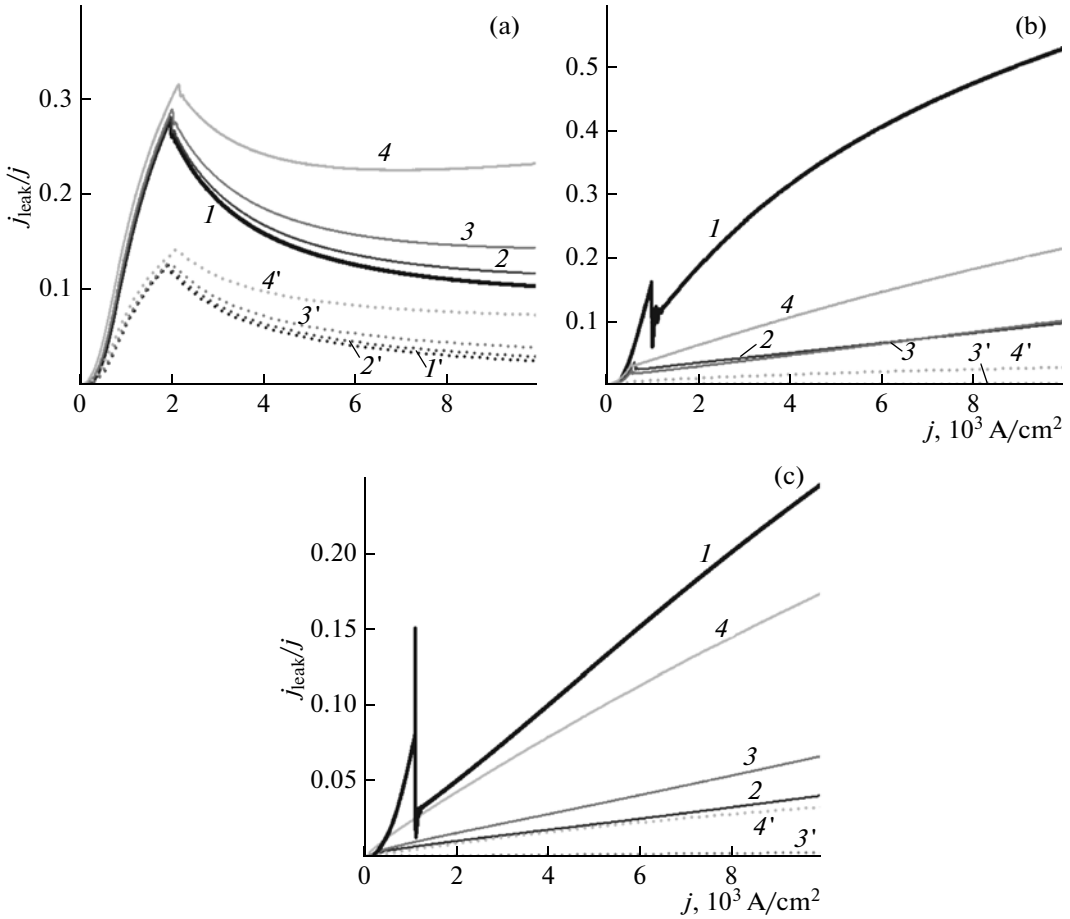

Fig. 2. Dependences of the normalized (solid lines) electron and (dotted lines) hole leakage currents on the current density through the structure in the lasing mode for heterostructures in the (a) InGaAs/GaAs, (b) InGaAsP/InP, and (c) InGaAs/InP systems at capture times of (*1'*, *1*) 0, (*2'*, *2*) 1, (*3'*, *3*) 3, and (*4'*, *4*) 10 ps ($k_{th} = 40$ cm^{-1}, $\varepsilon_s = 10^{-12}$ cm^2, and $\Gamma = 0.01$).

m_{vlt}, and m_{vht}) masses) for quaternary ($A_xB_{1-x}C_yD_{1-y}$), ternary ($A_xB_{1-x}C$), and binary (AB) compounds were approximated based on experimental and theoretical data according to [15]. The electron (μ_n) and hole (μ_p) mobilities were taken from the database [16]. When calculating the band structure, the potential-well depths in the conduction (ΔE_c) and valence (ΔE_v) bands were calculated according to [8]. The interpolation data for $Ga_{0.30}In_{0.70}As_{0.65}P_{0.35}$, $In_{0.2}Ga_{0.8}As$, $In_{0.53}Ga_{0.47}As$, GaAs, and InP compounds are listed in Table 1. The mobilities in the emitter layers are given in Table 2.

Figure 1 shows the calculated energy-band diagrams and positions of the Fermi quasi-levels for electrons (F_n) and holes (F_p). The emitters were assumed to be doped with acceptors to the concentration $N_a = 2 \times 10^{18}$ cm^{-3} and with donors to the concentration $N_d = 5 \times 10^{17}$ cm^{-3}. The weakly doped ($N_d = 5 \times 10^{16}$ cm^{-3}) layers 100 nm thick are adjacent to the QWs. In a structure with relatively shallow QWs (Fig. 1a), the ΔF_{wn} and ΔF_{wp} values, which characterize the inhomogeneous excitation of the QWs and barrier regions, do not exceed the thermal energy kT, and the excitation levels of all QWs are almost identical. In structures with lasing wavelengths of 1.31 and 1.55 μm (Figs. 1b and 1c), the ΔF_{wn} and ΔF_{wp} values exceed kT; in addition, these structures are characterized by significant inhomogeneous QW excitation and short capture times (~1 ps or shorter). Calculation of the latter structure under similar conditions but with carrier capture disregarded indicates a significant voltage drop in the QW region (Fig. 1d) due to the high ohmic resistance of the barrier regions with low carrier concentrations.

The results presented in Fig. 2 were obtained in the dynamic mode with the application of a pump current linearly increasing from 0 to 10 kA/cm^2 in 100 ns. The time scale in Fig. 2 is replaced with the scale of the corresponding injection-current density. A short transient process occurred after the onset of lasing. The relaxation oscillations strongly affected only the leakage currents calculated with the processes of carrier

capture by QWs neglected. Afterwards, the lasing became quasi-steady-state.

The InGaAs/GaAs structure has a low injection efficiency near the threshold (Fig. 2a); however, the fraction of leakage currents j_{leak} may decrease after the onset of lasing. The reason is that the carrier concentrations in the QWs in the lasing mode are fairly stable near the threshold level, the population of the barrier regions (which determines the leakage currents) barely changes for short capture times, and injection into the QWs increases proportionally to the induced-recombination rate. Beginning with a certain current value, the fraction of the leakage currents increases again. The leakage currents in the conduction band are higher than those in the valence band because of a higher electron mobility. The leakage currents can be reduced to an acceptable level by introducing blocking layers of wide-gap materials [17, 18]. These layers must be as thin as possible to exclude elimination of the waveguide mode as a result of their antiwaveguide effect.

The InGaAsP/InP and InGaAs/InP structures exhibit similar dependences of the leakage currents, which increase with an increase in the injection current (Figs. 2b and 2c). After the onset of lasing, this increase in only slowed (the jump in the dependence at the threshold is caused by the lasing-onset delay). When the threshold is several times exceeded, the leakage currents may reach several percent. In the InGaAs/InP structure with deeper QWs, the leakage currents are lower than those in the InGaAsP/InP structure by a factor of about 2. The current dependences of the leakage coefficient, which are calculated for zero capture times, differ significantly from the set of curves obtained at different τ_{cn} and τ_{cp} values. The reason is that calculation of the energy-band diagrams without regard for carrier capture by QWs leads to significant overestimation of the voltage drop on the ohmic resistance of the active region (Figs. 1c, 1d).

The multiple excess of the thermal energy by the homojunction potential barrier can be considered as a qualitative criterion of smallness of the leakage currents. For the heterostructures under study, the potential barriers $U = E_g - (F_e - F_h) \approx E_g - hc/\lambda$ at 300 K were found to be 6, 15, and $21kT$, respectively; this series correlates with the successive decrease (from the first to the third structure) in the leakage currents.

4. CONCLUSIONS

We developed a dynamic distributed diffusion–drift model of laser heterostructures, which takes into account the processes of carrier capture by QWs. The leakage currents were calculated for different QW-waveguide laser structures with lasing wavelengths of 0.98, 1.31, and 1.55 μm. It was shown that significant inhomogeneous excitation of the QWs in the InGaAsP/InP (1.31 μm) and InGaAs/InP (1.55 μm) structures occurs at capture times less than 1 ps. At the lasing threshold the leakage currents were estimated to be 35–45% for InGaAs/GaAs (0.98 μm), less than 5% for InGaAsP/InP (1.31 μm), and less than 1% for InGaAs/InP (1.55 μm). The leakage currents in the structures with deep QWs increase with an increase in the injection current and may reach several percent at a multiply exceeded threshold.

ACKNOWLEDGMENTS

This study was supported by the Belarusian Republican Foundation for Fundamental Research, project no. F12R-107.

REFERENCES

1. V. Ya. Aleshkin, A. A. Dubinov, B. N. Zvonkov, K. E. Kudryavtsev, and A. N. Yablonskii, in *Proceedings of the All-Russia Symposium on Nanophysics and Nanoelectronics* (Nizh. Novgorod, 2012), vol. 1, p. 241.
2. A. Yu. Leshko, A. V. Lyutetskii, N. A. Pikhtin, G. V. Skrynnikov, Z. N. Sokolova, I. S. Tarasov, and N. V. Fetisova, Semiconductors **34**, 1397 (2000).
3. Z. N. Sokolova, I. S. Tarasov, and L. V. Asryan, Semiconductors **45**, 1494 (2011).
4. S. G. Mulyarchik, *Numerical Simulation of Microelectronic Structures* (Universitetskoe, Minsk, 1989) [in Russian].
5. H. Hirayama, Y. Miyake, and M. Asada, IEEE J. Quantum Electron **28**, 68 (1992).
6. N. Tessler and G. Eistenstein, IEEE J. Quantum Electron. **29**, 1586 (1993).
7. A. A. Afonenko, V. K. Kononenko, and I. S. Manak, *Theory of Semiconductor Lasers* (Belorus. Gos. Univ., Minsk, 1995) [in Russian].
8. C. G. Chris, van de Walle, Phys. Rev. B **39**, 1871 (1989).
9. D. V. Ushakov, V. K. Kononenko, and I. S. Manak, J. Appl. Spectrosc. **66**, 820 (1999).
10. D. V. Ushakov and I. S. Manak, J. Appl. Spectrosc. **74**, 892 (2007).
11. J. A. Brum and G. Bastard, Phys. Rev. B **33**, 1420 (1986).
12. M. V. Vergeles and I. A. Merkulov, Sov. Phys. Semicond. **26**, 999 (1992).
13. L. V. Danilov and G. G. Zegrya, Tech. Phys. Lett. **39**, 255 (2013).
14. V. Ya. Aleshkin, A. A. Dubinov, L. V. Gavrilenko, Z. F. Krasil'nik, D. I. Kuritsyn, D. I. Kryzhkov, and S. V. Morozov, Semiconductors **46**, 917 (2012).
15. I. Vurgaftman, J. R. Meyer, and L. R. Ram-Mohan, J. Appl. Phys. **89**, 5815 (2001).
16. http://www.ioffe.rssi.ru/SVA/NSM/Semicond/index.html
17. D. V. Ushakov and V. K. Kononenko, Quantum Electron. **38**, 1001 (2008).
18. A. E. Zhukov, N. V. Kryzhanovskaya, M. V. Maximov, A. Yu. Egorov, M. M. Pavlov, F. I. Zubov, and L. V. Asryan, Semiconductors **45**, 530 (2011).

Translated by Yu. Sin'kov